Metabolic Engineering Communications 22 (2026) e00273

Contents lists available at ScienceDirect

Metabolic Engineering Communications

journal homepage: www.elsevier.com/locate/mec

Engineering *Pseudomonas taiwanensis* for efficient chorismate-based production of mono- and dihydroxybenzoates

Franziska Kofler [a], Tobias Schwanemann [a,b,1], Nadine Teófilo da Silva [a], Nick Wierckx [a,*], Benedikt Wynands [a]

[a] Institute of Bio- and Geosciences, IBG-1: Biotechnology, Forschungszentrum Jülich GmbH, 52425, Jülich, Germany
[b] iAMB – Institute of Applied Microbiology, ABBt – Aachen Biology and Biotechnology, RWTH Aachen University, Worringerweg 1, 52074, Aachen, Germany

A B S T R A C T

Aromatics have many important applications in modern society but are traditionally produced in non-sustainable processes from fossil resources. Whole-cell biocatalysis bears great potential to provide a variety of aromatics from renewable carbon sources, thereby offering a more sustainable alternative. In this context, chorismate, the end product of the shikimate pathway, is an important biosynthetic hub compound that serves as precursor of a multitude of industrially relevant aromatics. Here, we screened several pathways for chorismate-derived bioproduction of five different mono- and dihydroxybenzoates in tyrosine-overproducing *Pseudomonas taiwanensis* GRC3Δ5-TYR1. Subsequently, twelve different modifications targeting the bifunctional chorismate mutase/prephenate dehydratase PheA were screened to reduce flux from chorismate to phenylalanine and tyrosine, thereby further enhancing the production of 2-hydroxy- and 2,3-dihydroxybenzoate without causing an auxotrophy. An auxotrophic Δ*pheA* strain served as benchmark control. Most promising modifications were subsequently also evaluated for 3-hydroxy-, 4-hydroxy- and 2,5-dihydroxybenzoate production demonstrating increased yields. Replacing the native *pheA* gene with the unmodified homolog from *Escherichia coli* was the most beneficial, enabling an increased production of up to 38.2% when combined with *attTn7*::P_{14g}-*SmCH-IV*. With this modification, the highest production was achieved for 4-hydroxybenzoate resulting in titers of 3.59 mM and a yield of 20.9% (Cmol/Cmol) from glucose. However, the impact of the respective *pheA* modification varies with the applied production module, further emphasizing the strong interplay with the production host's metabolism.

1. Introduction

Aromatic compounds are essential to our modern life with a plethora of important applications, such as the production of pharmaceuticals, agrochemicals, polymers and plastics, or in food industry (Lee and Wendisch, 2017; Wu et al., 2018). Currently, the majority of aromatics is produced in petrochemical processes, which are associated with environmental pollution and the dependence on non-renewable fossil resources (Fiorentino et al., 2019). Providing bio-based alternatives to produce these commodity chemicals is of great importance to society in order to achieve sustainability (Yang et al., 2021). To that regard, microbial catalysis can be applied to obtain aromatics from renewable carbon sources at mild reaction conditions (Huccetogullari et al., 2019; Braga and Faria, 2020).

Although there are numerous publications available reporting efficient biosynthesis of various aromatic compounds (Wu et al., 2018; Huccetogullari et al., 2019), these are typically based on strains that were optimized for only one specific target product (Averesch and Krömer, 2018). Production of a variety of related products has been demonstrated (Kallscheuer and Marienhagen, 2018), but different production modules can yield orders of magnitude variations in production efficiencies, even when deriving from the same precursor in the same chassis. Engineering competent platform strains suitable for the production of several related molecules with high efficiency will help to reduce strain engineering costs and to promote the desired expansion of a bio-based industry enabling more standardized production processes (Noda et al., 2016).

Due to their high tolerance to organic solvents and aromatic compounds mediating robustness during production of harmful chemicals as well as their metabolic diversity enabling the utilization of various substrates, Pseudomonads such as *P. taiwanensis* VLB120 are particularly suitable for a broad range of biotechnological applications (Heipieper et al., 2007; Blank et al., 2008; Schwanemann et al., 2020; Bitzenhofer et al., 2021). In previous studies, genome-reduced *P. taiwanensis* VLB120 strains were already engineered for the production of phenylalanine- and tyrosine-derived aromatics (Wynands et al. 2018, 2019, 2023; Otto

* Corresponding author.
E-mail address: n.wierckx@fz-juelich.de (N. Wierckx).
[1] Present address: Tobias Schwanemann: iAMB – Institute of Applied Microbiology, ABBt – Aachen Biology and Biotechnology, RWTH Aachen University, Worringerweg 1, 52074 Aachen, Germany.

https://doi.org/10.1016/j.mec.2026.e00273
Received 16 January 2026; Accepted 25 January 2026
Available online 3 February 2026

et al. 2019, 2020). In this context, the deletion of *pobA, hpd, quiC, quiC1*, and *quiC2* (= Δ5) resulted in increased product titers by preventing degradation of aromatics and shikimate pathway intermediates (Wynands et al., 2018). The deletion of the pyruvate kinase-encoding *pykA* and implementation of a point mutation (P148L) in AroF-1, resulted in increased precursor supply and debottlenecked carbon flux into the shikimate pathway. Additional implementation of point mutations in the anthranilate synthase TrpE (P290S) and the bifunctional chorismate mutase/prephenate dehydratase PheA (T310I) reduced tryptophan biosynthesis and increased phenylalanine and tyrosine formation for derived phenol production (Wierckx et al., 2008; Wynands et al., 2018).

A chorismate platform strain is particularly interesting because a plethora of different biotechnologically relevant compounds can be derived from it including bulk and fine chemicals (Malik, 1979; Colquhoun et al., 2010; Huccetogullari et al., 2019). Among others, different phenolic acids can be produced from chorismate (Kumar and Goel, 2019), including three mono-hydroxybenzoates (2-, 3-, and 4-) and 2,3-

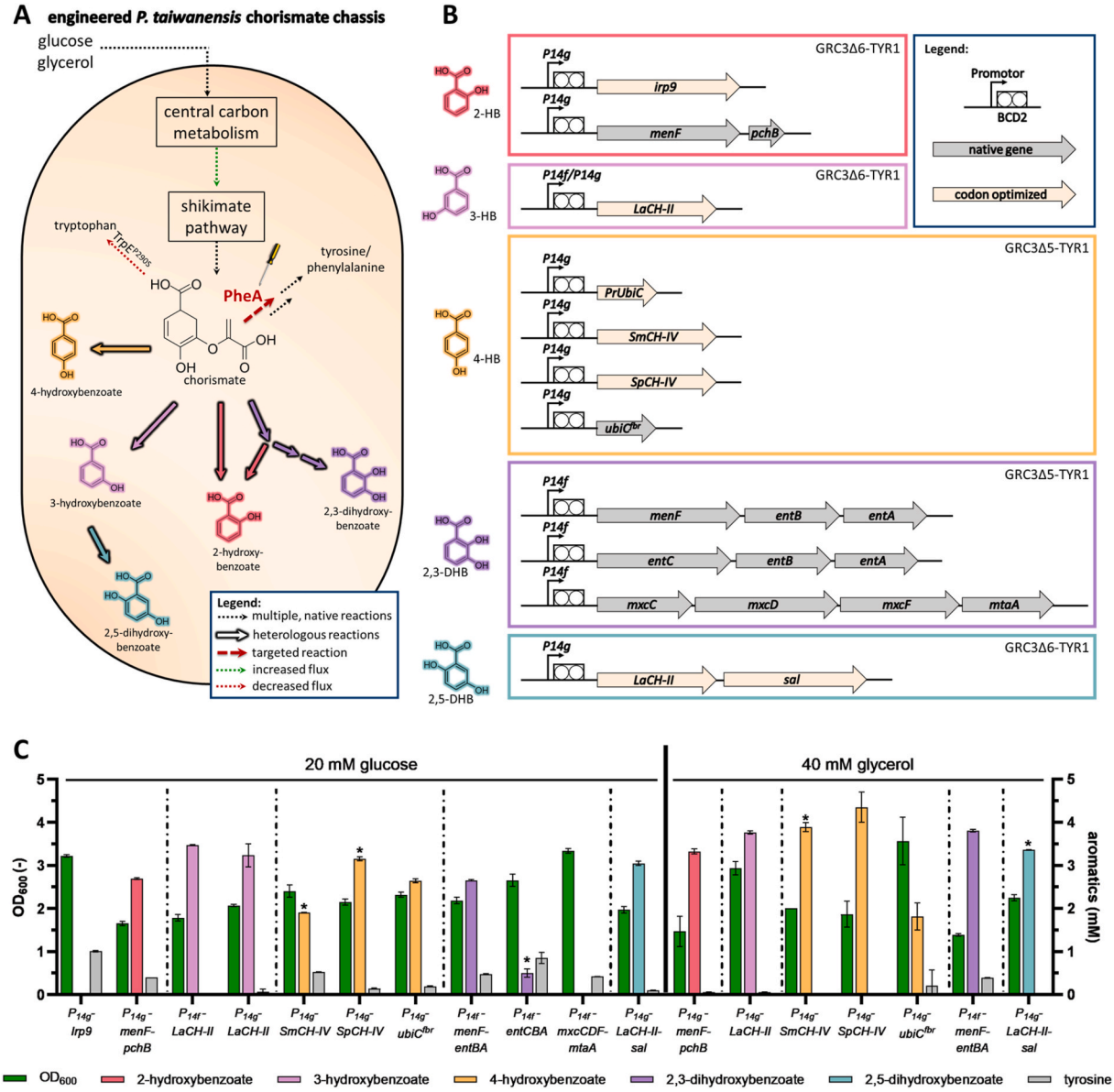

Fig. 1. *Pseudomonas taiwanensis* VLB120 as host for chorismate-derived hydroxybenzoate production. Schematic illustration of biosynthetic pathways in engineered *P. taiwanensis* strain (A) equipped with different production modules for chorismate-derived (di)hydroxybenzoate production (B). Production modules were designed to contain a translational coupler (BCD2) (Zobel et al., 2015), containing two ribosome binding sites upstream of the first pathway gene. Performance of the respective production modules in GRC3Δ5-TYR1 (4-hydroxy- & 2,3-dihydroxybenzoate) or GRC3Δ6-TYR1 (2-hydroxy-; 3-hydroxy-; 2,5-dihydroxybenzoate) grown on 20 mM glucose or 40 mM glycerol (C). To ensure carbon depletion, strains were cultivated for 96 h (on glucose) or 196 h (on glycerol). Error bars indicate standard deviation of biological replicates, with n = 3 except for graphs marked with an asterisk (*) where outliers were removed (n = 2). Please note that some of the error bars are hardly visible due to small standard deviations. For raw data including outliers, see supplementary data. Abbreviations: 2-HB, 2-hydroxybenzoate; 3-HB, 3-hydroxybenzoate; 4-HB, 4-hydroxybenzoate; 2,3-DHB, 2,3-dihydroxybenzoate; 2,5-DHB, 2,5-dihydroxybenzoate; PEP, phosphoenolpyruvate; E4P, erythrose 4-phosphate; AroF-1^{P148L}, DAHP synthase; EntA, 2,3-dihydro-2,3-dihydroxybenzoate dehydrogenase; EntB, enterobactin synthase component B; EntC, isochorismate synthase; Irp9, salicylate synthetase; LaCH-II, chorismatase; MenF, isochorismate synthase; MxcC, 2,3-dihydro-2,3-dihydroxybenzoate dehydrogenase; MxcD, isochorismate synthase; MxcF, isochorismatase; MtaA, 4′-phosphopantetheinyl transferase; PchB, isochorismate pyruvate lyase; PheA, bifunctional chorismate mutase/prephenate dehydratase; PrUbiC, chorismate lyase; Sal, 3-hydroxybenzoate 6-hydroxylase; SmCH-IV, chorismatase; SpCH-IV, chorismatase; TrpE^{P290S}, anthranilate synthase; UbiC^{fbr}, chorismate lyase.

and 2,5-dihydroxybenzoate that can be used e.g., as preservatives in food, cosmetics, and pharmaceutics as well as precursors of plastics and fibers (Dong et al., 2001; Franck and Stadelhofer, 2012; Huccetogullari et al., 2019; Kalinowska et al., 2021).

In this study, we demonstrate the efficient production of five different mono- and dihydroxybenzoates in a *P. taiwanensis* "CHOR" platform engineered for increased chorismate availability. The previously engineered tyrosine-overproducing strain *P. taiwanensis* GRC3Δ5-TYR1 (= Δ*pobA,* Δ*hpd,* Δ*quiC,* Δ*quiC1*, Δ*quiC2, trpE*^{P290S}*, aroF-1*^{P148L}, Δ*pykA*) (Wynands et al., 2023) was further modified to increase chorismate availability for derived heterologous production. As previous work already increased the metabolic flux into the shikimate pathway upstream of chorismate, we here aimed at reducing the drain on chorismate by decreasing the chorismate mutase activity of PheA without causing a phenylalanine and tyrosine auxotrophy (Molina-Henares et al., 2009). We evaluated 12 different variants of *pheA* to achieve a fine-tuned balance of chorismate availability between heterologous bioproduction and the flux towards phenylalanine and tyrosine required for cell viability. These strains were compared to the performance of an auxotrophic Δ*pheA* strain.

2. Results & discussion

2.1. Pathway evaluation for the production of different chorismate-derived hydroxybenzoates

In previous studies, genome-reduced *P. taiwanensis* strains with increased flux into the shikimate pathway were already established for the production of tyrosine- and phenylalanine-derived aromatics (Otto et al. 2019, 2020; Wynands et al. 2019, 2023). Based on the tyrosine-overproducing strain *P. taiwanensis* GRC3Δ5-TYR1 (Δ5, *trpE*^{P290S}, *aroF-1*^{P148L}, Δ*pykA*) (Wynands et al., 2023) we aimed to establish a platform strain for the efficient production of chorismate-derived mono- and dihydroxybenzoates.

In this context, production pathways for 2-hydroxy-, 3-hxydroxy-, 4-hydroxy, 2,3-dihydroxy-, and 2,5-dihydroxybenzoate (Fig. S1) were implemented in separate strains utilizing chorismate as common precursor (Fig. 1A). For some of these compounds, multiple production modules were evaluated as the catalytic performance of the selected pathway enzymes can significantly affect production. All production modules were cloned into mini-Tn7 delivery plasmids (pBG42 or pBG14f_FRT_Kan), equipped with a strong synthetic promotor (either P_{14g} or P_{14f}) and a BCD2 element, enabling targeted integration into the chromosomal Tn7 attachment site (*attTn7*) and strong constitutive expression (Zobel et al., 2015; Ackermann et al., 2021) (Fig. 1B). For initial pathway characterization the 4-hydroxy- and 2,3-dihydroxybenzoate modules were integrated into GRC3Δ5-TYR1. Those for 2-hydroxy-, 3-hydroxy- and 2,5-dihydroxybenzoate were integrated into strain GRC3Δ6-TYR1, an identical strain with additional Δ*benABCD* modification. This was done as we could associate *benABCD* encoding the benzoate dioxygenase and dihydroxycyclohexadiene carboxylate dehydrogenase to the disappearance of supplemented 2-hydroxybenzoate (salicylate) and to some extent also 3-hydroxybenzoate (Fig. S2). Respective production strains with native wild-type *pheA* (here denoted as *Pt_pheA*^{WT}) were all screened for their endpoint production performance in minimal salt medium containing 20 mM glucose and selected strains in medium containing 40 mM glycerol as carbon source in 24-well microtiter plates (Fig. 1C–Table 1).

The introduction of production modules into the TYR1 chassis resulted in product titers up to 3.47 ± 0.01 mM (*attTn7*::P_{14f}-*LaCH-II*) from 20 mM glucose. Overall, only the intended product compounds and no unexpected byproduct formation were detected, indicating no undesirable side activities of the implemented production enzymes. However, the efficiency of production differed strongly depending on the applied production module. For instance, despite successful application of Irp9 in other organisms where titers up to 3.72 g L^{-1} were achieved (Kerbarh et al., 2005; Kallscheuer and Marienhagen, 2018; Chen et al., 2024), GRC3Δ6-TYR1 *attTn7*::P_{14g}-*irp9* showed no significant 2-hydroxybenzoate production here in *P. taiwanensis*. The integration of *attTn7*::P_{14g}-*menF-pchB* (Noda et al., 2016; Schwanemann et al., 2023) however resulted in 2.69 ± 0.02 mM 2-hydroxybenzoate. Similarly, only one of the three implemented production modules for 2,3-dihydroxybenzoate (*attTn7*::P_{14f}-*menF-entBA*) showed efficient production up to 2.65 ± 0.01 mM. Moreover, despite the reported native and mutation-mediated product inhibition resistance of SmCH-IV, SpCH-IV, and UbiC^{fbr} (Grüninger et al., 2019; Jha et al., 2019) 4-hydroxybenzoates titers varied significantly (p-values below 0.005) from 1.90 ± 0.01 mM to 3.15 ± 0.05 mM. For *attTn7*::P_{14g}-*PrUbiC*, highly variable results were obtained suggesting an unstable construct (Fig. S3).

When extending the 3-hydroxybenzoate production module by addition of *sal* for the production of 2,5-dihydroxybenzoate, final titers reduced from 3.47 ± 0.01 mM 3-hydroxybenzoate to 3.04 ± 0.05 mM 2,5-dihydroxybenzoate and correlated with slight tyrosine

Table 1
Parameters of hydroxybenzoate production in GRC3Δ5-TYR1 or GRC3Δ6-TYR1 harboring the respective production modules integrated into the Tn7 attachment site (*attTn7*).

Production module	Carbon source	OD_{600}	Product (mM)	Yield Cmol %	Tyrosine (mM)	References production module
P_{14g}-*MenF-PchB* (2-HB)	glucose	1.7 ± 0.0	2.69 ± 0.02	15.7 ± 0.1	0.40 ± 0.00	Noda et al. (2016), Schwanemann et al. (2023)
	glycerol	1.5 ± 0.4	3.32 ± 0.06	19.4 ± 0.3	0.05 ± 0.01	
P_{14g}-*Irp9* (2-HB)	glucose	3.2 ± 0.0	0.01 ± 0.00	0.1 ± 0.0	1.01 ± 0.01	Kerbarh et al. (2005), Kallscheuer and Marienhagen (2018), Chen et al. (2024)
P_{14f}-*LaCH-II* (3-HB)	glucose	1.8 ± 0.1	3.47 ± 0.01	20.3 ± 0.1	0.00 ± 0.00	Grüninger et al. (2019)
	glycerol	2.9 ± 0.2	3.76 ± 0.04	21.9 ± 0.2	0.05 ± 0.01	
P_{14g}-*LaCH-II* (3-HB)	glucose	2.1 ± 0.0	3.23 ± 0.27	18.9 ± 1.6	0.06 ± 0.07	
P_{14g}-*SmCH-IV* (4-HB)	glucose	2.4 ± 0.1	1.90 ± 0.01	11.1 ± 0.1	0.52 ± 0.01	
	glycerol	2.0 ± 0.0	3.89 ± 0.10	22.7 ± 0.6	0.00 ± 0.00	
P_{14g}-*SpCH-IV* (4-HB)	glucose	2.2 ± 0.1	3.15 ± 0.05	18.4 ± 0.3	0.14 ± 0.01	
	glycerol	1.9 ± 0.3	4.35 ± 0.35	25.4 ± 2.1	0.00 ± 0.00	
P_{14g}-*ubiC*^{fbr} (4-HB)	glucose	2.3 ± 0.1	2.64 ± 0.04	15.4 ± 0.3	0.19 ± 0.01	Jha et al. (2019)
	glycerol	3.6 ± 0.6	1.81 ± 0.31	10.6 ± 1.8	0.21 ± 0.36	
P_{14f}-*MenF-EntBA* (2,3-DHB)	glucose	2.2 ± 0.3	2.65 ± 0.01	15.5 ± 0.1	0.47 ± 0.01	Dahm et al. (1998), Bin and Pawelek (2024)
	glycerol	2.2 ± 0.1	3.80 ± 0.03	22.6 ± 0.2	0.30 ± 0.01	
P_{14f}-*entCBA* (2,3-DHB)	glucose	2.7 ± 0.1	0.50 ± 0.10	2.9 ± 0.6	0.85 ± 0.13	Sun et al. (2014)
P_{14f}-*mxcCDF_mtaA* (2,3-DHB)	glucose	3.3 ± 0.1	0.00 ± 0.00	0.0 ± 0.0	0.42 ± 0.00	Silakowski et al. (2000), Korp et al. (2018)
P_{14g}-*LaCH-II-Sal* (2,5-DHB)	glucose	1.9 ± 0.0	3.04 ± 0.05	17.8 ± 0.3	0.10 ± 0.00	Wang et al. (2021)
	glycerol	2.3 ± 0.1	3.36 ± 0.01	19.6 ± 0.0	0.00 ± 0.00	

accumulation. This might be related to altered expression patterns due to the integration of a second gene into the expression cassette. However, no 3-hydroxybenzoate was detected indicating sufficient activity of Sal and no competition between the pathways.

Despite the expectation of negligible toxicity effects of the produced compounds in the titer ranges achieved here, notable discrepancies in the yields of different products and even between enzymes catalyzing the same reactions were observed. This phenomenon may be explained by varied enzymatic properties (K_m, k_{cat}) exhibited by the respective production modules. However, the determination of enzymatic properties is typically conducted *in vitro* under conditions that differ from the *in vivo* environment. Consequently, predicting the most effective production module is often challenging, necessitating the screening of numerous modules.

In general, accumulation of up to 0.52 ± 0.01 mM tyrosine was observed on glucose. On glycerol, tyrosine accumulation was reduced in five out of seven cases to a minimum (≤0.05 ± 0.01 mM) while 4-hydroxybenzoate production increased up to 4.35 ± 0.35 mM (*attTn7*::P_{14g}-SpCH-IV) thereby improving production yields from maximal 20.3 ± 0.1 up to 25.4 ± 2.1% (Cmol/Cmol). Of note, considerably higher titers of 8.3 g L^{-1} 4-hydroxybenzoate were previously reported for *Corynebacterium glutamicum*, but with supplementation of yeast extract and aromatic amino acids (Doke et al., 2023). Even without considering the supplementation of complex medium components these titers correlate with carbon molar yields similar to the production described here using *P. taiwanensis* in fully minimal medium. Overall, these results indicate that, especially on glucose, more chorismate is converted into phenylalanine and tyrosine than urgently required for cell growth. Moreover, a strong disparity in performance was observed for the different production strains. Especially the distinct efficiency differences between the 4-hydroxybenzoate production modules highlight the impact of the respective enzymes on pathway regulation and the competition.

2.2. Engineering chorismate mutase activity of PheA to enhance chorismate availability for bioproduction

Similarly to the implemented mutation in *trpE* for decreased flux to tryptophan (Wierckx et al., 2008; Wynands et al., 2018), we aimed to modify *pheA* to further decrease the drain on chorismate by limiting the flux to phenylalanine and tyrosine. In contrast to *E. coli* and *C. glutamicum* bearing multiple chorismate mutases, PheA is the host's only known chorismate mutase (and prephenate dehydratase) catalyzing the conversion of chorismate to prephenate.

To determine the efficiency of production processes, it is imperative to account for the supplementation of additional components, including amino acids or yeast extract during yield calculations (Yook and Alper, 2025). To prevent phenylalanine auxotrophy caused by a *pheA* knockout, chorismate mutase activity should be reduced but not fully eliminated in order to avoid the co-feed of costly amino acids or their precursors. Hence, we aimed to implement mutations into the chorismate mutase domain of *P. taiwanensis* to reduce its activity. Most studies addressing the activity of bacterial chorismate mutase focus on *in vitro* characterization with PheA from *E. coli* (Liu et al., 1996; Zhang et al. 1998, 2000). Therefore, in addition to integrating amino acid substitutions into the native *pheA* locus of *P. taiwanensis*, we also either completely or partially exchanged the native *pheA* gene with that from *E. coli*. We thus generate a chimeric protein consisting of the well-characterized chorismate mutase domain from *E. coli* fused to the host's native prephenate dehydratase and regulatory domain (here denoted as *hybrid_pheA*^{WT}), as well as a fully native version (*Pt_pheA*^{WT}) and a full *E. coli* version (*Ec_pheA*^{WT}). Subsequently, point mutations in E52 were implemented into the respective *pheA* variants, given that alterations at this position attenuate chorismate mutase activity in *E. coli* (Liu et al., 1996). Similarly, two further point mutations reported for *E. coli* (I81L,V85L) (Lassila et al., 2005) were transferred into the host's *pheA* (I81L, C85I). An amino acid exchange within the regulatory domain of Ec_PheA (W338L) was also introduced to alter chorismate mutase activity (Zhang et al., 2000). This point mutation was previously introduced to native PheA of *P. aeruginosa* PA1201 (corresponding to amino acid exchange W323L) causing 23% increased phenazine-1-carboxylic acid production (Jin et al., 2015). Taking the high structural similarity between PheA from *E. coli*, *P. aeruginosa,* and *P. taiwanensis* into account (Fig. S4), mainly differing in the length of the domain linkers, the respective mutations were implemented both in *Ec_pheA* and in *Pt_pheA*. Besides adaptations targeting protein activity, the start codon ATG was exchanged through the less-preferred GTG aiming for decreased expression levels instead. An overview over the different PheA variants and the estimated impact on chorismate mutase activity can be found in Table S1. To benchmark the full production potential, *pheA* was also deleted as a control to prevent flux from chorismate towards phenylalanine and tyrosine entirely.

Modifications significantly reducing chorismate mutase activity were expected to show reduced growth due to a bradytrophy for these amino acids. Due to its capability to convert phenylalanine into tyrosine (Arias-Barrau et al., 2004), both auxotrophies can be rescued through nutritional complementation with phenylalanine. However, the deletion of *pheA* was reported to be very challenging in *P. putida* KT2440 despite the use of complex LB medium and supplementation of phenylpyruvate (Kuepper et al., 2015; Yu et al., 2016) consequently resulting in growth impairment that could be only restored by supplementation of 1–5 mM phenylpyruvate or 1 mM phenylalanine. Our initial efforts to delete *pheA* in *P. taiwanensis* were repeatedly unsuccessful despite the supplementation of phenylalanine or phenylpyruvate to the LB medium, screening for tiny colonies (Kuepper et al., 2015; Yu et al., 2016), and introducing additional plasmid-encoded copies of *pheA*. The deletion of *pheA* was only achieved by integrating a tetracycline resistance cassette (Δ*pheA*::*tetA*) for selection. The resulting strain showed reduced growth on LB agar, which was also observed for some of the other *pheA* modifications. Colony forming units were only visible after two days incubation and in some cases (*hybrid_pheA* variants) differed significantly in size.

To characterize growth phenotypes of the individual *pheA* modifications in the background of GRC3Δ6-TYR1 the respective non-producing strains were grown using the Growth Profiler in minimal medium on glucose without phenylalanine supplementation (Fig. 2A). To assess the impact on aromatics production, GRC3Δ6-TYR1 strains with the different *pheA* modifications were equipped with P_{14g}-*menF-pchB* at the *attTn7*-site and characterized for their growth in the same medium (Fig. 2B). Growth Profiler data obtained for growth under phenylalanine supplementation are depicted in Fig. S5. Although the deletion of *pheA* was confirmed by whole genome sequencing, we unexpectedly observed growth for GRC3Δ6-TYR1Δ*pheA* even without phenylalanine supplementation (Fig. S5). This could be explained if there was another chorismate mutase present in *P. taiwanensis*. For *P. aeruginosa,* a second chorismate mutase and a periplasmic "hidden overflow pathway" to phenylalanine was postulated (Fiske et al., 1983; Calhoun et al., 2001). However, to the best of our knowledge, no second prephenate dehydratase is present in *P. taiwanensis,* required to compensate for the deletion of *pheA*. The observed growth of GRC3Δ6-TYR1Δ*pheA* was very slow, especially after integration of the production module, and could be complemented by phenylalanine supplementation. Therefore, the strain remains a reliable reference due to significantly reduced conversion of chorismate.

To investigate the effect on production, all *pheA*-engineered strains with either P_{14g}-*menF-pchB* or P_{14f}-*menF-entBA* integrated into the chromosome (*attTn7*), were grown in 24-well microtiter plates on glucose and evaluated for 2-hydroxy- or 2,3-dihydroxybenzoate production (Fig. 2C and D). Subsequently, most promising *pheA* variants identified for P_{14g}-*menF-pchB* and P_{14f}-*menF-entBA* were applied in combination with the remaining production modules and evaluated under the same process conditions (Fig. 2E).

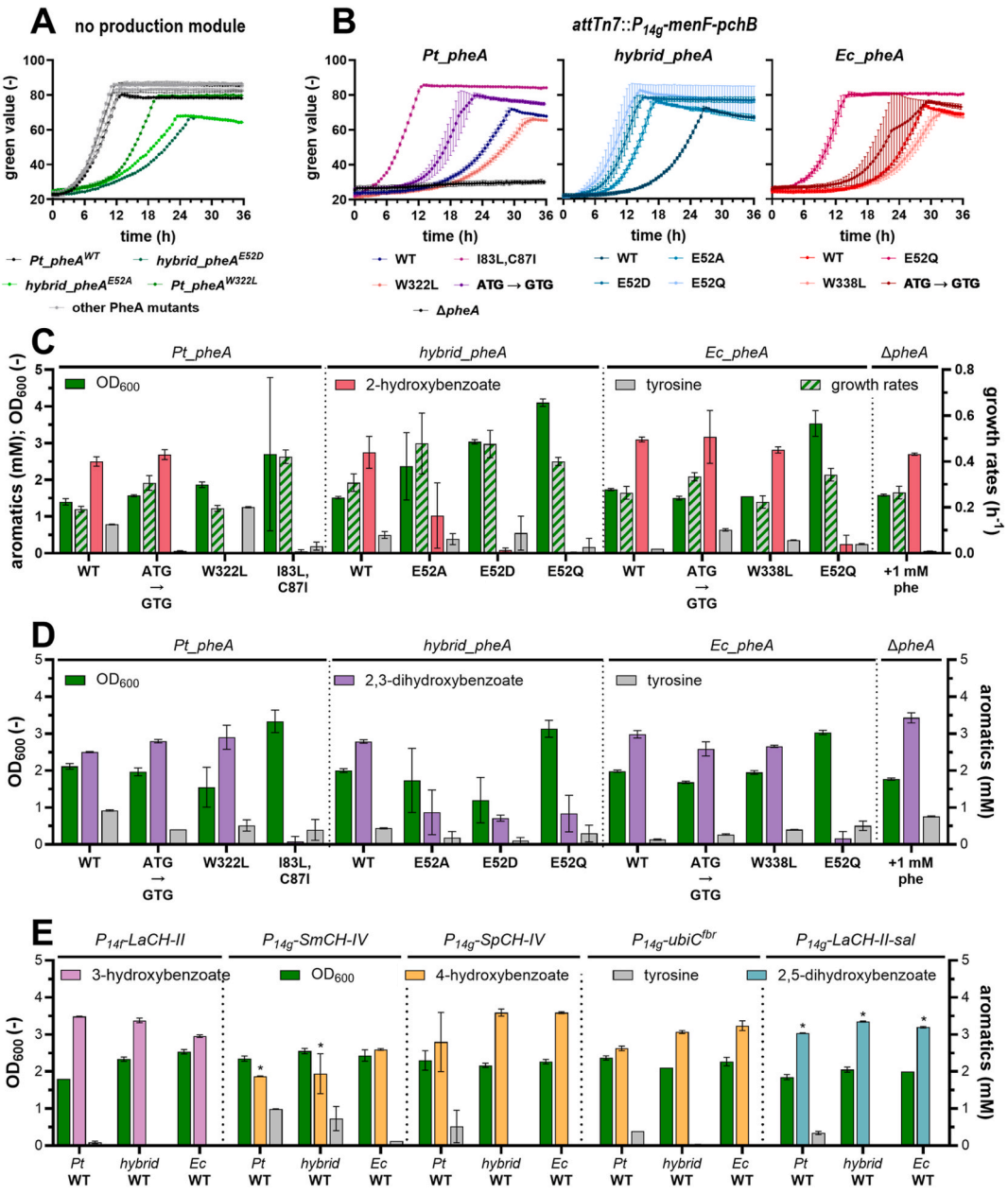

Fig. 2. Impact of *pheA* mutations on growth and hydroxybenzoate production. GRC3Δ6-TYR1 strains with different *pheA* modifications without (A with n = 4) or with the production module *attTn7*::P_{14g}-*menF-pchB* (B with n = 8) were cultivated in two-fold-buffered MSM containing 20 mM glucose without phenylalanine. Resulting growth curves (B) were used for the calculation of OD_{600}-equivalents and growth rates displayed in C. The complete set of 12 *pheA* modifications in GRC3Δ6-TYR1-*attTn7*::P_{14g}-*menF-pchB* (C) or GRC3Δ5-TYR1-*attTn7*::P_{14f}-*menF-entBA* (D), and selected *pheA* variants combined with the remaining production modules *attTn7*::P_{14f}-*LaCH-II*, *attTn7*::P_{14g}-*SmCH-IV*, *attTn7*::P_{14g}-*SpCH-IV*, *attTn7*::P_{14g}-*ubiC*^{fbr}, or *attTn7*::P_{14g}-*LaCH-II-sal* (E) were cultured in 24-well microtiter plates using two-fold-buffered MSM with 20 mM glucose. To enable sufficient growth of the phenylalanine auxotrophic Δ*pheA* strains, 1 mM phenylalanine was supplemented to the respective cultures. To ensure carbon depletion, strains were cultivated for 96 h. Error bars indicate standard deviation of biological replicates, with n = 3 (C–E) except for graphs marked with an asterisk (*) where outliers were removed (n = 2). Please note that some of the error bars are hardly visible due to small standard deviations. For raw data including outliers, see supplementary data. Abbreviations: Ec, *E. coli*; Pt, *P. taiwanensis*; phe, phenylalanine; WT, wild type.

Enzyme engineering was performed to balance product accumulation and cell growth. Indeed, three *pheA* mutants led to decreased growth rates compared to the wild type, as observed for the strains bearing *Pt_pheA*^{W322L} (0.29 ± 0.02 h^{-1}), *hybrid_pheA*^{E52A} (0.18 ± 0.01 h^{-1}), or *hybrid_pheA*^{E52D} (0.17 ± 0.01h^{-1}), which grew slowest compared to the *Pt_pheA*^{WT} strain (0.41 ± 0.01 h^{-1}) (Fig. 2A). Most *pheA* mutants however showed overall similar growth (0.40 ± 0.03 h^{-1}) as the wild type. Under the assumption that slower growth indicates a more severe bradytrophy and consequently elevated chorismate availability, the slow growing strains were anticipated to produce the highest chorismate-derived hydroxybenzoate titers. Yet, as enzyme engineering was done in an already highly optimized strain to exploit its full potential, the scope for enhancement is narrow. However, when combining these *pheA* variants with a 2-hydroxybenzoate production module (*attTn7*::P_{14g}-*menF-pchB*), production was instead drastically reduced. Overall, the producing strains showed much higher variations in their growth (Fig. 2B). Growth rates were increased in the abovementioned *pheA* mutants, but only after a prolonged lag phase. However, in other *pheA* mutants like the strain bearing *Ec_pheA*^{WT}, production was increased significantly (p-value = 0.002) from 2.50 ± 0.13 mM

(*Pt_pheA*^{WT}) to 3.10 ± 0.06 mM 2-hydroxybenzoate. Enhanced 2-hydroxybenzoate production correlated with reduced tyrosine accumulation from 0.78 ± 0.01 mM (*Pt_pheA*^{WT}) to 0.12 ± 0.00 mM (*Ec_pheA*^{WT}). This corresponds to a 24.2% increased production and a carbon molar yield of 18.1 ± 0.4%. The deletion of *pheA* and supplementation of 1 mM phenylalanine also increased production to 2.70 ± 0.03 mM 2-hydroxybenzoate corresponding to a yield of 14.6 ± 0.7% (Cmol/Cmol). This shows the benefit of the more subtle *pheA* modifications, with the *Ec_pheA*^{WT} attaining a higher titer and yield without supplementation.

The same trends were observed for the production of 2,3-dihydroxybenzoate in the respective GRC3Δ5-TYR1 *pheA* mutants. Production was increased by up to 19.3% from initial 2.50 ± 0.02 mM (*Pt_pheA*^{WT}) to 2.79 ± 0.05 mM (*hybrid_pheA*^{WT}) and further up to 2.98 ± 0.10 mM (*Ec_pheA*^{WT}). Accumulation of tyrosine was decreased from 0.90 ± 0.02 mM (*Pt_pheA*^{WT}) to 0.13 ± 0.02 mM (*Ec_pheA*^{WT}). Contrary to our expectations, none of the tested point mutations that were previously shown to increase the K_M of the chorismate mutase domain enhanced production compared to the initial strain with wild type *Pt*_PheA. Instead, less severe mutations improved production significantly. This demonstrates the challenges regarding the transferability between *in vitro* and *in vivo* data. It also highlights the need to balance the competition between PheA-mediated flux to phenylalanine and tyrosine as natural end points of the metabolic pathway, and heterologous aromatics production modules. This further exemplifies the high complexity of the regulation and interaction between different metabolic routes especially in *Pseudomonas*' shikimate pathway.

It should be noted that in the Δ*pheA* strain, 2,3-dihydroxybenzoate production was further increased to 3.43 ± 0.14 mM with a carbon molar yield of 18.6 ± 0.7%. Despite the high similarity between both Δ*pheA* production strains, only differing in the target compound and the absence or presence of *benABCD,* significant differences of the overall production performances were observed. However, together with the unexpected growth of the non-producing Δ*pheA* strain even in absence of phenylalanine (Fig. S5), this further highlights the increasing difficulty of handling auxotrophic *pheA* mutant strains in Pseudomonads as also observed in previous studies (Kuepper et al., 2015; Yu et al., 2016). Overall, auxotrophic production strains such as GRC3Δ5-TYR1Δ*pheA-attTn7*::P_{14f}-*menF-entBA* come with benefits and disadvantages. Auxotrophies can provide higher product specificity or enable new approaches such as limiting fed-batch fermentations thereby avoiding inhibition patterns as described by Kuepper et al. (2015). However, the supplementation of the required compounds is cost-intensive and can lead to increased complexity of process design.

Subsequently to the comparison of the different *pheA* modifications, the three best performing strains expressing either *Pt_pheA*^{WT}, *hybrid_pheA*^{WT} (*P. taiwanensis* CHOR1), or *Ec_pheA*^{WT} (*P. taiwanensis* CHOR2) were further evaluated with the remaining hydroxybenzoate production modules to confirm the general applicability of the chorismate chassis (Fig. 2E). For the three distinct 4-hydroxybenzoate-producing enzymes SmCH-IV, SpCH-IV, and UbiC^{fbr}, similar trends in production and tyrosine accumulation were observed. Depending on the respective production module, exchanging either solely the chorismate mutase domain or the whole gene led to relative increases of up to 38.2%. Thus, 4-hydroxybenzoate production was increased from 1.88 ± 0.00 mM (base strain) to 2.60 ± 0.02 mM (*Ec_pheA*^{WT}) using *attTn7*::P_{14g}-*SmCH-IV*. The highest 4-hydroxybenzoate production was achieved with module *attTn7*::P_{14g}-*SpCH-IV* in combination with *Ec_pheA*^{WT}. In this case, production was elevated from 2.80 ± 0.80 mM (of the base strain) up to 3.59 ± 0.03 mM, corresponding to a carbon molar yield of 20.9 ± 0.2%. This slightly exceeds the 4-hydroxybenzoate yield of 19.0% (Cmol/Cmol) that was previously achieved for a similar *P. taiwanensis* production strain with a much longer production pathway that proceeds via tyrosine and *p*-coumarate as intermediates (Lenzen et al., 2019).

Surprisingly, when *hybrid_pheA*^{WT} or *Ec_pheA*^{WT} were tested in combination with *LaCH-II,* 3-hydroxybenzoate production decreased. Of note, production of 3-hydroxybenzoate by the base strain with wild type *Pt*_PheA was highest (3.48 ± 0.01 mM) of all tested products with only low concentrations of accumulating tyrosine (0.09 ± 0.03 mM). Thus, the potential for additional optimization through engineering of *pheA* was likely already minimized. Considering LaCH-II's initial high performance, adjusting PheA likely led to increased metabolic burden without the benefit of generating a higher chorismate availability for 3-hydroxybenzoate production. However, when *LaCH-II* was combined with *sal*, the PheA exchanges did increase 2,5-dihydroxybenzoate production from 3.03 ± 0.01 mM (*Pt*_PheA) to 3.35 ± 0.02 mM (*hybrid*_PheA) and 3.20 ± 0.02 mM (*Ec*_PheA), again highlighting the interplay between PheA-modified chassis and production module.

The PheA modifications in *P. taiwanensis* resulted high carbon molar yields from a fully mineral medium. Similar or higher yields compared to literature were obtained for 4-, 2,3-, and 2,5-dihydroxybenzoate. Despite the beneficial impact of exchanging *pheA*, for 2-hydroxbenzoate yields are lower than achieved with *E. coli* (47.7% Cmol/Cmol) (Noda et al., 2016) and *C. glutamicum* (24.5% Cmol/Cmol) (Doke et al., 2023). However, in both cases, the highest benefit on production was achieved when transitioning from small scale cultivation to bioreactors. In small-scale batch cultures, lower titers corresponding to carbon molar yields of 11.3% (*E. coli*) and 16.1% (*C. glutamicum*) were reported. In this context, the here reported yields reached with *P. taiwanensis* in fully mineral medium depict good production which might be further increased when optimizing the production process. Titers can likewise be increased by providing more substrate in batch or fed-batch bioreactor cultivations (Lenzen et al., 2019; Otto et al., 2019).

2.3. Growth and production characterization

For further characterization of growth and production parameters, selected strains were cultivated in shake flasks to monitor growth and production over time (Figs. 3 and 4, Table 2).

In accordance with the growth rates on glucose observed in the PheA variants with and without production modules (Fig. 3), the substrate uptake rates and final OD_{600} of these strains were, at most, only marginally different from the control. At the same time, the production of both hydroxybenzoates was increased regarding product titers and yields by 17.8% (2-hydroxybenzoate) and 15.6% (2,3-dihydroxy-benzoate) comparing *Pt_pheA*^{WT} and *Ec_pheA*^{WT}, without negatively affecting the overall production time of about 29 h. At this time, glucose and gluconate were fully consumed and hydroxybenzoate production was mostly completed. However, even after this point, tyrosine concentrations increased up to 0.56 ± 0.01 mM for the base strain bearing *attTn7*::P_{14g}-*menF-pchB* and 0.62 ± 0.01 mM bearing *attTn7*::P_{14f}-*menF-entBA* resulting in product specificities of 86 ± 1% and 84 ± 0%. This can be explained by the conversion of phenylalanine or other precursors to tyrosine that cannot be detected with the applied HPLC method. Independent from the time of tyrosine production, its accumulation shows that PheA is converting more chorismate into prephenate than required to maintain cell vitality. This tyrosine accumulation is much less pronounced in the *pheA* mutants and even eliminated (0.01 ± 0.00 mM) in the strains bearing *Ec_pheA*^{WT} resulting in 100% specificity in all respective cultures displaying a major benefit for downstream processing. The combination of increased production combined with reduced tyrosine accumulation indicates that the respective PheA variants show a decrease in activity to the extent that a lower proportion of chorismate is available for phenylalanine and tyrosine biosynthesis without significantly affecting growth, while improving chorismate supply for heterologous aromatics production.

When cultivated on 40 mM glycerol, overall slower growth and longer lag phases were observed as compared to growth on glucose. Maximal OD_{600} was reached between 56 h and 72 h depending on the strain. At this time, glycerol was depleted and production was completed in most strains. Even though no tyrosine accumulation was observed for strains bearing *Pt_pheA*^{WT} when grown on glycerol, increased

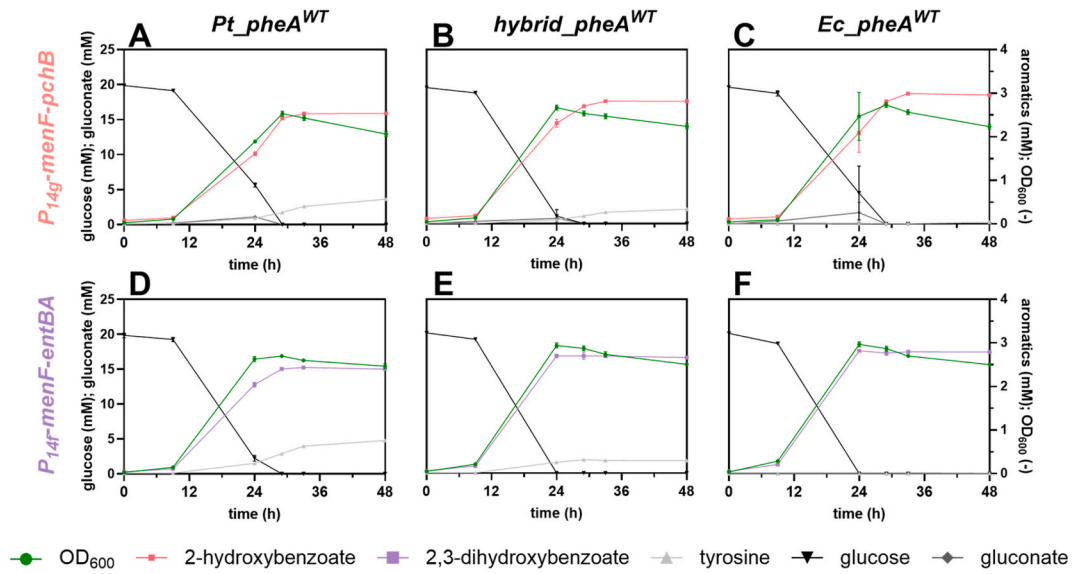

Fig. 3. Shake flask cultivation of *P. taiwanensis* TYR1 (*Pt_pheA*^{WT}) (A, D), *P. taiwanensis* CHOR1 (*hybrid_pheA*^{WT}) (B, E), or *P. taiwanensis* CHOR2 (*Ec_pheA*^{WT}) (C, F) bearing either *attTn7*::P_{14g}-*menF-pchB* (A–C) or *attTn7*::P_{14f}-*menF-entBA* (D–F) in two-fold-buffered MSM with 20 mM glucose. Error bars indicate the standard deviation of replicates (n = 3) although some are diminutive in size.

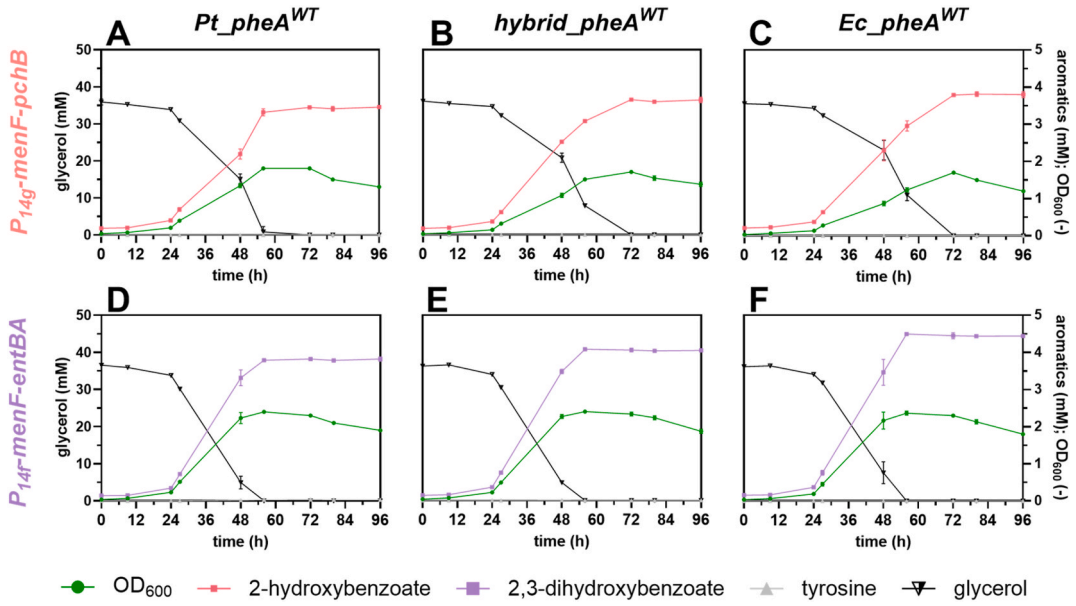

Fig. 4. Shake flask cultivation of *P. taiwanensis* TYR1 (*Pt_pheA*^{WT}) (A, D), *P. taiwanensis* CHOR1 (*hybrid_pheA*^{WT}) (B, E), or *P. taiwanensis* CHOR2 (*Ec_pheA*^{WT}) (C, F) bearing either *attTn7*::P_{14g}-*menF-pchB* (A–C) or *attTn7*::P_{14f}-*menF-entBA* (D–F) in two-fold-buffered MSM with 40 mM glycerol. Error bars indicate the standard deviation of replicates (n = 3), although some are diminutive in size.

Worttrennung production was detected for strains expressing *hybrid_pheA*^{WT} or *Ec_pheA*^{WT} respectively. For 2-hydroxybenzoate production, titers could be increased from 3.27 ± 0.03 mM to 3.58 ± 0.02 mM, giving yields of 19.1 ± 0.2% (Cmol/Cmol) and 20.9 ± 0.1% (Cmol/Cmol) respectively. In case of 2,3-dihydroxybenzoate, the full exchange of *Pt_pheA*^{WT} to *Ec_pheA*^{WT} resulted in 18.9% increased production correlating to a final titer of 4.34 ± 0.05 mM and yield of 25.3 ± 0.3% (Cmol/Cmol). This is significantly higher compared to production from glucose. Increased aromatics production and decreased growth rates when using glycerol as carbon source are a commonly observed phenomenon for *de novo* production in *Pseudomonas sp.* as described in multiple previous publications (Lenzen et al., 2019; Otto et al., 2019; Wynands et al., 2023). It is probably related to a downregulated flux through the Entner-Doudoroff pathway and the tricarboxylic acid cycle preventing carbon loss in form of CO_2 or accumulation of acidic by-products (Nikel et al., 2014).

3. Conclusion

The primary hypothesis of this study was that modulation of the chorismate mutase enzyme activity enables improved production of chorismate-derived aromatics by creating a phenylalanine bradytrophy. Hence, the effect of PheA mutations on growth was tested with different mutants indeed having different bradytrophic severities. Too severe growth limitations had a negative effect on both production and growth, while less severe mutations did improve production. Out of 11 modifications, the highest benefit was observed for *Ec_pheA*^{WT} followed by *hybrid_pheA*^{WT}. There, tyrosine accumulation was reduced correlating

Table 2
Production parameters of selected 2-hydroxybenzoate or 2,3-dihydroxybenzoate producers.

Production strain	Carbon source	max OD_{600}	Product (mM)	Yield Cmol%	Specificity (%)
P. taiwanensis TYR1-*attTn7::P_{14g}-menF-pchB* (2-HB)	glucose	2.5 ± 0.1 (29 h)	2.44 ± 0.02 (33 h)	14.2 ± 0.1 (33 h)	86 ± 1 (33 h)
	glycerol	1.8 ± 0.0 (56 h)	3.27 ± 0.03 (72 h)	19.1 ± 0.2 (72 h)	98 ± 0 (72 h)
P. taiwanensis CHOR1-*attTn7::P_{14g}-menF-pchB* (2-HB)	glucose	2.7 ± 0.1 (24 h)	2.70 ± 0.01 (33 h)	15.7 ± 0.1 (33 h)	92 ± 0 (33 h)
	glycerol	1.7 ± 0.0 (72 h)	3.48 ± 0.04 (72 h)	20.3 ± 0.2 (72 h)	100 ± 0 (72 h)
P. taiwanensis CHOR2- *attTn7::P_{14g}-menF-pchB* (2-HB)	glucose	2.7 ± 0.1 (29 h)	2.88 ± 0.06 (33 h)	16.8 ± 0.4 (33 h)	100 ± 0 (33 h)
	glycerol	1.7 ± 0.0 (72 h)	3.58 ± 0.02 (72 h)	20.9 ± 0.1 (72 h)	100 ± 0 (72 h)
P. taiwanensis TYR1-*attTn7::P_{14f}-menF-entBA* (2,3-DHB)	glucose	2.7 ± 0.0 (29 h)	2.36 ± 0.01 (29 h)	13.8 ± 0.1 (29 h)	84 ± 0 (29 h)
	glycerol	2.4 ± 0.0 (56 h)	3.65 ± 0.02 (56 h)	21.3 ± 0.1 (56 h)	92 ± 0 (56 h)
P. taiwanensis CHOR1- *attTn7::P_{14f}-menF-entBA* (2,3-DHB)	glucose	2.9 ± 0.1 (24 h)	2.64 ± 0.04 (24 h)	15.4 ± 0.2 (24 h)	92 ± 1 (24 h)
	glycerol	2.4 ± 0.0 (56 h)	3.94 ± 0.04 (56 h)	23.0 ± 0.2 (56 h)	99 ± 0 (56 h)
P. taiwanensis CHOR2-*attTn7::P_{14f}-menF-entBA* (2,3-DHB)	glucose	3.0 ± 0.1 (24 h)	2.76 ± 0.04 (24 h)	16.1 ± 0.2 (24 h)	100 ± 0 (24 h)
	glycerol	2.4 ± 0.1 (56 h)	4.34 ± 0.05 (56 h)	25.3 ± 0.3 (56 h)	100 ± 0 (56 h)

with increased hydroxybenzoate production. Thus, chorismate-derived aromatics production was successfully increased by up to 38.2% (*attTn7::P_{14g}-SmCH-IV*), depending on the production module. Extended fermentation experiments might be performed in the future, exploring the impact of different cultivation volumes and systems. Together with increased carbon feeds, this could enable process optimization and production titers while current experiments prioritized carbon molar yields. Overall, this study demonstrates the added value of the here engineered *P. taiwanensis* CHOR chassis strains, while also emphasizing the need to balance metabolic fluxes between different production modules and essential amino acid biosynthesis, on the background of the overall metabolic flux varied by feeding glucose vs. glycerol (Fig. 5).

4. Experimental procedures

4.1. Media and culture conditions

E. coli and *P. taiwanensis* VLB120 strains were grown in lysogeny broth (LB) medium containing 10 g L^{-1} tryptone, 5 g L^{-1} yeast extract, and 5 g L^{-1} sodium chloride either in liquid medium or on solid plates supplemented with 15 g L^{-1} agar (Carl Roth). Cultivation of *E. coli* and *P. taiwanensis* was performed at 37 and 30 °C, respectively. Selectivity during cloning procedures and pre-cultures was ensured using final concentrations of 50 mg L^{-1} kanamycin sulfate (Carl Roth), 100 mg L^{-1} ampicillin (Carl Roth), 10 mg L^{-1} (in liquid) or 25 mg L^{-1} (in solid media) gentamicin (Carl Roth), and 200 mg L^{-1} streptomycin sulfate (Carl Roth). For the *pheA* replacement by the *tetA* marker, 30 mg L^{-1} tetracycline hydrochloride (Carl Roth) was added to the medium. In case of gentamicin and streptomycin, the applied concentrations were

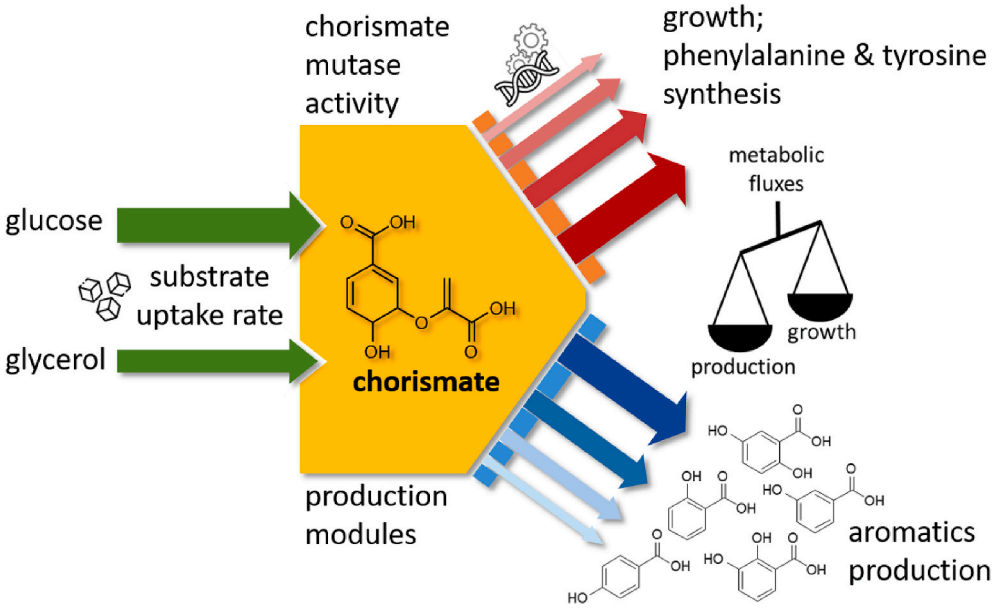

Fig. 5. Schematic depiction of aromatics production depending on balancing of metabolic fluxes into chorismate production and downstream pathways.

lowered to 10 mg L^{-1} and 50 mg L^{-1} respectively for cultivation of *E. coli*. Selection of *Pseudomonas* after patch mating was ensured by adding 25 mg L^{-1} Irgasan (Sigma Aldrich). Production tests were performed using mineral salt medium (MSM) adapted from Hartmans et al. (1989) with a phosphate buffer capacity of 44.6 mM K_2HPO_4 and 27.2 mM NaH_2PO_4 supplemented with either 20 mM D-(+)-glucose monohydrate (Carl Roth) or 40 mM glycerol (Carl Roth). Production modules were integrated into the chromosome together with a selectable antibiotic marker. The respective antibiotics were added to the pre-cultures only but not to the production media to relieve the antibiotic burden. For the cultivation of strains harboring the Δ*pheA* modification, phenylalanine was supplemented to the medium as indicated for the individual experiment.

Screenings for the highest production were performed in small-scale cultures deploying System Duetz 24-well microtiter plates (CR1424a, EnzyScreen), filled with 1.5 mL medium and sealed with sandwich covers (CR1224b, EnzyScreen). System Duetz plates were shaken at 300 rpm with a throw of 50 mm.

For cultivation in a Growth Profiler 960, 200 µL MSM was inoculated to an OD_{600} of 0.1 in greyish-white 96-half-deep-well microtiter plates with flat transparent bottoms (CR1496dg, EnzyScreen). After sealing with sandwich covers (CR1296b, EnzyScreen), cultures were shaken at 225 rpm and a throw of 50 mm.

For a more detailed characterization of production over time, selected strains were cultivated using Erlenmeyer shake flasks filled with 10% (v/v) minimal salt medium and shaken at 200 rpm with a throw of 50 mm.

4.2. Plasmid cloning and strain engineering

Primers for cloning (Table S3), diagnostic PCRs, and Sanger sequencing were ordered from Eurofins Genomics as unmodified oligonucleotides. Gene fragments used for cloning were amplified using the Q5 High-Fidelity 2X Master Mix (New England Biolabs). Diagnostic PCRs were performed using the OneTaq Quick-Load 2X Master Mix with Standard Buffer (New England Biolabs) according to the manufacturer's instruction manual. Template colonies were prelyzed with alkaline PEG 200 according to Chomczynski and Rymaszewski (2006).

Plasmids (Table S4) were constructed as described in Table S5 using the NEBuilder HiFi DNA Assembly Master Mix (New England Biolabs) according to the vendor's protocol. Chemically competent *E. coli* PIR2 cells were transformed with the generated plasmids to enable plasmid amplification prior plasmid isolation using the Monarch Plasmid Miniprep Kit (New England Biolabs).

Codon optimization was done for *P. taiwanensis* VLB120 using the OPTIMIZER online tool (Puigbo et al., 2007) as outlined in Wynands et al. (2018). The associated coding sequences can be found in Table S6. The RBS calculator v2.1 was used to predict or control translation initiation rates for (synthetic) ribosome binding sites (Salis et al., 2009). Point mutations, allelic replacements, and deletions were introduced using the homologous recombination-based I-SceI system (Martínez-García and de Lorenzo, 2011) applying the workflow described in Wynands et al. (2018). The seamless deletion of *pheA* was not achieved after several attempts without a selection pressure. Therefore, the deletion of *pheA* was facilitated by the knock-in of a tetracycline resistance marker (Δ*pheA*:*tetA*). For the delivery of deletion/integration plasmids, the *Pseudomonas* recipient, the helping strain *E. coli* HB101 pRK2013, and the respective *E. coli* donor were patched for conjugation. In case of chromosomal integration of the production cassettes into the *attTn7* site of the *Pseudomonas* recipient, *E. coli* DH5α λpir pTNS1, providing the required transposase proteins *in trans*, was additionally added to the patch mating. Strains generated and used in this study are summarized in Table S7.

4.3. Analytic methods

Optical densities of cell cultures were measured at 600 nm (OD_{600}) using an Ultrospec 10 photometer (Biochrom). To monitor growth behavior, certain cultivations were performed using the Growth Profiler 960 (Enzyscreen), capturing bottom-up images of a 96-well plate with transparent bottom to determine the green value using the corresponding GP960Viewer software. The green value correlates with the optical density in a non-linear manner. To determine growth rates, the respective green values were subsequently converted into OD_{600} equivalents using the following function.

$$OD_{600}\ equivalent = a^*(gValue - gBlank)^b + c^*(gValue - gBlank)^d + e^*(gValue - gBlank)^f$$

$$a = 0.0014; b = 1.2; c = 0.0000025; d = 3; e = 4^*E^{-13}; f = 6.8$$
$$gBlank = 22.947$$

Growth rates were determined by applying exponential fits (with $R^2 \geq 0.95$) to the natural logarithmic values of the OD_{600} data points (≥3) and the respective time ranges.

Prior to quantification of substrates, metabolites, products and by-products, cell culture samples were centrifuged, filtered, and stored at −20°C. Samples were measured on a 1260 Infinity II HPLC system equipped with a 1260 DAD WR and 1260 RID (Agilent Technologies). Aromatic compounds were either analyzed using an ISAspher 100-5 C18 BDS column (4.0 × 250 mm, ISERA; P.N.: A111-C25S00) with guard column (ISERA; P.N.: A112-C25G30) or an InfinityLab Poroshell 120 EC-C18 column (3.0 × 150 mm, 2.7 µm, Agilent Technologies, P.N. 693975-302T) with guard column (Agilent Technologies; P.N.: 823750-911). Elution of the analytes occurred at 40°C using gradients of 0.1% (v/v) trifluoroacetic acid (TFA, Sigma-Aldrich) and acetonitrile (Th. Geyer) at a flow rate of 0.8 mL min^{-1} as described in Table S8 and Table S9. With increasing hydroxybenzoate concentrations, samples were acidified to a final concentration of 0.5% TFA prior injection on the Poroshell 120 EC-C18.

Glucose, gluconate and glycerol concentrations were measured using a Metab-AAC column (300 × 7.8 mm, ISERA; P.N.: A1BF-A1AA0N) equipped with a guard cartridge holder (ISERA, P.N.: AA13- 000005) and guard column (10 × 7.8 mm, ISERA; A1BF-A1AG0N). The analytes were eluted using a 20 min isocratic flow of 5 mM H_2SO_4 and 0.6 mL min^{-1} at 60 °C.

D-(+)-Glucose monohydrate (≥99.5%, Carl Roth), D-gluconic acid sodium salt (≥99% Sigma-Aldrich), glycerol (Chemsolute, ≥99%, Th. Geyer), L-tyrosine (≥99%, Sigma-Aldrich), 4-hydroxybenzoic acid (99%, Sigma-Aldrich), 3-hydroxybenzoic acid (99%, Sigma-Aldrich), 2-hydroxybenzoic acid (≥99.0%, Sigma-Aldrich), 2,3-dihydroxybenzoic acid (99%, Sigma Aldrich) and 2,5-dihydroxybenzoic acid (98%, Sigma Aldrich) served as authentic standards.

The calculated yields used the net product accumulation (maximum - initial concentration) and the measured carbon consumption for cultivations sampled over time. For initial screening experiments with endpoint determination, yields were calculated assuming full carbon consumption and no product transfer during inoculation. Where applicable, supplemented phenylalanine was considered in the carbon molar yield calculations as well (Yook and Alper, 2025).

All experiments were conducted with biological replicates as specified. Occasional analytical outliers were removed from the data sets as indicated. Errors indicate the standard deviation. Statistical significance was determined using a two-tailed, heteroscedastic *t*-test with a significance threshold of $p < 0.05$.

CRediT authorship contribution statement

Franziska Kofler: Investigation, Validation, Visualization, Writing – original draft, Writing – review & editing. **Tobias Schwanemann:**

Investigation, Writing – review & editing. **Nadine Teófilo da Silva:** Investigation. **Nick Wierckx:** Conceptualization, Funding acquisition, Supervision, Writing – review & editing. **Benedikt Wynands:** Conceptualization, Investigation, Supervision, Validation, Writing – review & editing.

Funding

We acknowledge funding from the German Federal Ministry of Education and Research (BMBF) for Bio4Mat-Pro BoostLab2-3 – SAVER2 (FKZ 031B1149DX) and the European Research Council for the project PROSPER (Grant No.: 101044949).

Declaration of competing interest

The authors declare that they have no known competing financial interests or personal relationships that could have appeared to influence the work reported in this paper.

Acknowledgements

We thank Sophia Feltes (IBG-1: Biotechnology, Forschungszentrum Jülich) for her support with the OD_{600} calibration for Growth Profiler experiments and Astrid Wirtz (IBG-1: Biotechnology, Forschungszentrum Jülich) for her kind assistance with analytical questions.

Appendix A. Supplementary data

Supplementary data to this article can be found online at https://doi.org/10.1016/j.mec.2026.e00273.

Data availability

The data are provided in the supplementary files.

References

Ackermann, Y.S., Li, W.-J., de Hipt, L.O., Niehoff, P.-J., Casey, W., Polen, T., Köbbing, S., Ballerstedt, H., Wynands, B., O'Connor, K., 2021. Engineering adipic acid metabolism in Pseudomonas putida. Metab. Eng. 67, 29–40. https://doi.org/10.1016/j.ymben.2021.05.001.

Arias-Barrau, E., Olivera, E.R., Luengo, J.M., Fernández, C., Galán, B., García, J.L., Díaz, E., Minambres, B., 2004. The homogentisate pathway: a central catabolic pathway involved in the degradation of L-phenylalanine, L-tyrosine, and 3-hydroxyphenylacetate in *Pseudomonas putida*. J. Bacteriol. 186 (15), 5062–5077. https://doi.org/10.1128/jb.186.15.5062-5077.2004.

Averesch, N.J., Krömer, J.O., 2018. Metabolic engineering of the shikimate pathway for production of aromatics and derived compounds—present and future strain construction strategies. Front. Bioeng. Biotechnol. 6, 32. https://doi.org/10.3389/fbioe.2018.00032.

Bin, X., Pawelek, P.D., 2024. Evidence of isochorismate channeling between the *Escherichia coli* enterobactin biosynthetic enzymes EntC and EntB. Protein Sci. 33 (8), e5122. https://doi.org/10.1002/pro.5122.

Bitzenhofer, N.L., Kruse, L., Thies, S., Wynands, B., Lechtenberg, T., Rönitz, J., Kozaeva, E., Wirth, N.T., Eberlein, C., Jaeger, K.-E., 2021. Towards robust Pseudomonas cell factories to harbour novel biosynthetic pathways. Essays Biochem. 65 (2), 319–336. https://doi.org/10.1042/EBC20200173.

Blank, L.M., Ionidis, G., Ebert, B.E., Bühler, B., Schmid, A., 2008. Metabolic response of *Pseudomonas putida* during redox biocatalysis in the presence of a second octanol phase. FEBS J. 275 (20), 5173–5190. https://doi.org/10.1111/j.1742-4658.2008.06648.x.

Braga, A., Faria, N., 2020. Bioprocess optimization for the production of aromatic compounds with metabolically engineered hosts: recent developments and future challenges. Front. Bioeng. Biotechnol. 8, 96. https://doi.org/10.3389/fbioe.2020.00096.

Calhoun, D.H., Bonner, C.A., Gu, W., Xie, G., Jensen, R.A., 2001. The emerging periplasm-localized subclass of AroQ chorismate mutases, exemplified by those from *Salmonella typhimurium* and *Pseudomonas aeruginosa*. Genome Biol. 2, 1–16. https://doi.org/10.1186/gb-2001-2-8-research0030.

Chen, C., Gao, C., Hu, G., Wei, W., Wang, X., Wen, J., Chen, X., Liu, L., Song, W., Wu, J., 2024. Rational and semirational approaches for engineering salicylate production in *Escherichia coli*. ACS Synth. Biol. 13 (11), 3563–3575. https://doi.org/10.1021/acssynbio.4c00366.

Chomczynski, P., Rymaszewski, M., 2006. Alkaline polyethylene glycol-based method for direct PCR from bacteria, eukaryotic tissue samples, and whole blood. Biotechniques 40 (4), 454–458. https://doi.org/10.2144/000112149.

Colquhoun, T.A., Schimmel, B.C., Kim, J.Y., Reinhardt, D., Cline, K., Clark, D.G., 2010. A petunia chorismate mutase specialized for the production of floral volatiles. Plant J. 61 (1), 145–155. https://doi.org/10.1111/j.1365-313X.2009.04042.x.

Dahm, C., Müller, R., Schulte, G., Schmidt, K., Leistner, E., 1998. The role of isochorismate hydroxymutase genes *entC* and *menF* in enterobactin and menaquinone biosynthesis in *Escherichia coli*. Biochimica et Biophysica Acta (BBA)-General Subjects 1425 (2), 377–386. https://doi.org/10.1016/S0304-4165(98)00089-0.

Doke, M., Kishida, M., Hirata, Y., Nakano, M., Horita, M., Nonaka, D., Mori, Y., Fujiwara, R., Kondo, A., Noda, S., 2023. Hydroxybenzoic acid production using metabolically engineered Corynebacterium glutamicum. Synthetic Biol. Eng. 1 (2), 10010. https://doi.org/10.35534/sbe.2023.10010.

Dong, D., Jiang, S., Ni, Y., Jiang, B., 2001. Syntheses and properties of thermotropic copolyesters of p-hydroxybenzoic acid. Eur. Polym. J. 37 (3), 611–617. https://doi.org/10.1016/S0014-3057(00)00123-3.

Fiorentino, G., Zucaro, A., Ulgiati, S., 2019. Towards an energy efficient chemistry. Switching from fossil to bio-based products in a life cycle perspective. Energy 170, 720–729. https://doi.org/10.1016/j.energy.2018.12.206.

Fiske, M., Whitaker, R., Jensen, R., 1983. Hidden overflow pathway to L-phenylalanine in *Pseudomonas aeruginosa*. J. Bacteriol. 154 (2), 623–631. https://doi.org/10.1128/jb.154.2.623-631.1983.

Franck, H.-G., Stadelhofer, J.W., 2012. Industrial Aromatic Chemistry: Raw Materials· Processes· Products. Springer Science & Business Media.

Grüninger, M.J., Buchholz, P.C., Mordhorst, S., Strack, P., Müller, M., Hubrich, F., Pleiss, J., Andexer, J.N., 2019. Chorismatases–the family is growing. Org. Biomol. Chem. 17 (8), 2092–2098. https://doi.org/10.1039/C8OB03038C.

Hartmans, S., Smits, J., Van der Werf, M., Volkering, F., De Bont, J., 1989. Metabolism of styrene oxide and 2-phenylethanol in the styrene-degrading *Xanthobacter* strain 124X. Appl. Environ. Microbiol. 55 (11), 2850–2855. https://doi.org/10.1128/aem.55.11.2850-2855.1989.

Heipieper, H.J., Neumann, G., Cornelissen, S., Meinhardt, F., 2007. Solvent-tolerant bacteria for biotransformations in two-phase fermentation systems. Appl. Microbiol. Biotechnol. 74, 961–973. https://doi.org/10.1007/s00253-006-0833-4.

Huccetogullari, D., Luo, Z.W., Lee, S.Y., 2019. Metabolic engineering of microorganisms for production of aromatic compounds. Microb. Cell Fact. 18, 1–29. https://doi.org/10.1186/s12934-019-1090-4.

Jha, R.K., Narayanan, N., Pandey, N., Bingen, J.M., Kern, T.L., Johnson, C.W., Strauss, C. E., Beckham, G.T., Hennelly, S.P., Dale, T., 2019. Sensor-enabled alleviation of product inhibition in chorismate pyruvate-lyase. ACS Synth. Biol. 8 (4), 775–786. https://doi.org/10.1021/acssynbio.8b00465.

Jin, K., Zhou, L., Jiang, H., Sun, S., Fang, Y., Liu, J., Zhang, X., He, Y.-W., 2015. Engineering the central biosynthetic and secondary metabolic pathways of Pseudomonas aeruginosa strain PA1201 to improve phenazine-1-carboxylic acid production. Metab. Eng. 32, 30–38. https://doi.org/10.1016/j.ymben.2015.09.003.

Kalinowska, M., Gołębiewska, E., Świderski, G., Męczyńska-Wielgosz, S., Lewandowska, H., Pietryczuk, A., Cudowski, A., Astel, A., Świsłocka, R., Samsonowicz, M., 2021. Plant-derived and dietary hydroxybenzoic acids—A comprehensive study of structural, anti-/pro-oxidant, lipophilic, antimicrobial, and cytotoxic activity in MDA-MB-231 and MCF-7 cell lines. Nutrients 13 (9), 3107. https://doi.org/10.3390/nu13093107.

Kallscheuer, N., Marienhagen, J., 2018. *Corynebacterium glutamicum* as platform for the production of hydroxybenzoic acids. Microb. Cell Fact. 17, 1–13. https://doi.org/10.1186/s12934-018-0923-x.

Kerbarh, O., Ciulli, A., Howard, N.I., Abell, C., 2005. Salicylate biosynthesis: overexpression, purification, and characterization of Irp9, a bifunctional salicylate synthase from *Yersinia enterocolitica*. J. Bacteriol. 187 (15), 5061–5066. https://doi.org/10.1128/jb.187.15.5061-5066.2005.

Korp, J., Winand, L., Sester, A., Nett, M., 2018. Engineering pseudochelin production in *Myxococcus xanthus*. Appl. Environ. Microbiol. 84 (22). https://doi.org/10.1128/AEM.01789-18 e01789-e01718.

Kuepper, J., Dickler, J., Biggel, M., Behnken, S., Jäger, G., Wierckx, N., Blank, L.M., 2015. Metabolic engineering of *Pseudomonas putida* KT2440 to produce anthranilate from glucose. Front. Microbiol. 6, 1310. https://doi.org/10.3389/fmicb.2015.01310.

Kumar, N., Goel, N., 2019. Phenolic acids: natural versatile molecules with promising therapeutic applications. Biotechnol. Rep. 24, e00370. https://doi.org/10.1016/j.btre.2019.e00370.

Lassila, J.K., Keeffe, J.R., Oelschlaeger, P., Mayo, S.L., 2005. Computationally designed variants of Escherichia coli chorismate mutase show altered catalytic activity. Protein Eng. Des. Sel. 18 (4), 161–163. https://doi.org/10.1093/protein/gzi015.

Lee, J.-H., Wendisch, V.F., 2017. Biotechnological production of aromatic compounds of the extended shikimate pathway from renewable biomass. J. Biotechnol. 257, 211–221. https://doi.org/10.1016/j.jbiotec.2016.11.016.

Lenzen, C., Wynands, B., Otto, M., Bolzenius, J., Mennicken, P., Blank, L.M., Wierckx, N., 2019. High-yield production of 4-hydroxybenzoate from glucose or glycerol by an engineered *Pseudomonas taiwanensis* VLB120. Front. Bioeng. Biotechnol. 7, 130. https://doi.org/10.3389/fbioe.2019.00130.

Liu, D.R., Cload, S.T., Pastor, R.M., Schultz, P.G., 1996. Analysis of active site residues in Escherichia coli chorismate mutase by site-directed mutagenesis. J. Am. Chem. Soc. 118 (7), 1789–1790. https://doi.org/10.1021/ja953151o.

Malik, V.S., 1979. Regulation of chorismate-derived antibiotic production. Adv. Appl. Microbiol. 25, 75–93. https://doi.org/10.1016/S0065-2164(08)70147-3.

Martínez-García, E., de Lorenzo, V., 2011. Engineering multiple genomic deletions in gram-negative bacteria: analysis of the multi-resistant antibiotic profile of *Pseudomonas putida* KT2440. Environ. Microbiol. 13 (10), 2702–2716. https://doi.org/10.1111/j.1462-2920.2011.02538.x.

Molina-Henares, M.A., García-Salamanca, A., Molina-Henares, A.J., De La Torre, J., Herrera, M.C., Ramos, J.L., Duque, E., 2009. Functional analysis of aromatic biosynthetic pathways in *Pseudomonas putida* KT2440. Microb. Biotechnol. 2 (1), 91–100. https://doi.org/10.1111/j.1751-7915.2008.00062.x.

Nikel, P.I., Kim, J., De Lorenzo, V., 2014. Metabolic and regulatory rearrangements underlying glycerol metabolism in *Pseudomonas putida* KT 2440. Environ. Microbiol. 16 (1), 239–254. https://doi.org/10.1111/1462-2920.12224.

Noda, S., Shirai, T., Oyama, S., Kondo, A., 2016. Metabolic design of a platform *Escherichia coli* strain producing various chorismate derivatives. Metab. Eng. 33, 119–129. https://doi.org/10.1016/j.ymben.2015.11.007.

Otto, M., Wynands, B., Lenzen, C., Filbig, M., Blank, L.M., Wierckx, N., 2019. Rational engineering of phenylalanine accumulation in Pseudomonas taiwanensis to enable high-yield production of trans-cinnamate. Front. Bioeng. Biotechnol. 7, 312. https://doi.org/10.3389/fbioe.2019.00312.

Otto, M., Wynands, B., Marienhagen, J., Blank, L.M., Wierckx, N., 2020. Benzoate synthesis from glucose or glycerol using engineered *Pseudomonas taiwanensis*. Biotechnol. J. 15 (11), 2000211. https://doi.org/10.1002/biot.202000211.

Puigbo, P., Guzmán, E., Romeu, A., Garcia-Vallvé, S., 2007. OPTIMIZER: a web server for optimizing the codon usage of DNA sequences. Nucleic Acids Res. 35 (Suppl. l_2), W126–W131. https://doi.org/10.1093/nar/gkm219.

Salis, H.M., Mirsky, E.A., Voigt, C.A., 2009. Automated design of synthetic ribosome binding sites to control protein expression. Nat. Biotechnol. 27 (10), 946–950. https://doi.org/10.1038/nbt.1568.

Schwanemann, T., Otto, M., Wierckx, N., Wynands, B., 2020. *Pseudomonas* as versatile aromatics cell factory. Biotechnol. J. 15 (11), 1900569. https://doi.org/10.1002/biot.201900569.

Schwanemann, T., Urban, E.A., Eberlein, C., Gätgens, J., Rago, D., Krink, N., Nikel, P.I., Heipieper, H.J., Wynands, B., Wierckx, N., 2023. Production of (hydroxy) benzoate-derived polyketides by engineered *Pseudomonas* with in situ extraction. Bioresour. Technol. 388, 129741. https://doi.org/10.1016/j.biortech.2023.129741.

Silakowski, B., Kunze, B., Nordsiek, G., Blöcker, H., Höfle, G., Müller, R., 2000. The myxochelin iron transport regulon of the myxobacterium *Stigmatella aurantiaca* Sg a15. Eur. J. Biochem. 267 (21), 6476–6485. https://doi.org/10.1046/j.1432-1327.2000.01740.x.

Sun, X., Lin, Y., Yuan, Q., Yan, Y., 2014. Biological production of muconic acid via a prokaryotic 2, 3-dihydroxybenzoic acid decarboxylase. ChemSusChem 7 (9), 2478–2481. https://doi.org/10.1002/cssc.201402092.

Wang, S., Fu, C., Liu, K., Cui, J., Hu, H., Wang, W., Zhang, X., 2021. Engineering a synthetic pathway for gentisate in *Pseudomonas chlororaphis* p3. Front. Bioeng. Biotechnol. 8, 622226. https://doi.org/10.3389/fbioe.2020.622226.

Wierckx, N.J., Ballerstedt, H., de Bont, J.A., de Winde, J.H., Ruijssenaars, H.J., Wery, J., 2008. Transcriptome analysis of a phenol-producing *Pseudomonas putida* S12 construct: genetic and physiological basis for improved production. J. Bacteriol. https://doi.org/10.1128/jb.01379-07.

Wu, F., Cao, P., Song, G., Chen, W., Wang, Q., 2018. Expanding the repertoire of aromatic chemicals by microbial production. J. Chem. Technol. Biotechnol. 93 (10), 2804–2816. https://doi.org/10.1002/jctb.5690.

Wynands, B., Kofler, F., Sieberichs, A., da Silva, N., Wierckx, N., 2023. Engineering a Pseudomonas taiwanensis 4-coumarate platform for production of para-hydroxy aromatics with high yield and specificity. Metab. Eng. 78, 115–127. https://doi.org/10.1016/j.ymben.2023.05.004.

Wynands, B., Lenzen, C., Otto, M., Koch, F., Blank, L.M., Wierckx, N., 2018. Metabolic engineering of Pseudomonas taiwanensis VLB120 with minimal genomic modifications for high-yield phenol production. Metab. Eng. 47, 121–133. https://doi.org/10.1016/j.ymben.2018.03.011.

Wynands, B., Otto, M., Runge, N., Preckel, S., Polen, T., Blank, L.M., Wierckx, N., 2019. Streamlined Pseudomonas taiwanensis VLB120 chassis strains with improved bioprocess features. ACS Synth. Biol. 8 (9), 2036–2050. https://doi.org/10.1021/acssynbio.9b00108.

Yang, L., Wang, X.-C., Dai, M., Chen, B., Qiao, Y., Deng, H., Zhang, D., Zhang, Y., de Almeida, C.M.V.B., Chiu, A.S., 2021. Shifting from fossil-based economy to bio-based economy: status quo, challenges, and prospects. Energy 228, 120533. https://doi.org/10.1016/j.energy.2021.120533.

Yook, S., Alper, H.S., 2025. Bioconversion yields must account for all carbon: hidden biases from complex media. Trends Biotechnol. https://doi.org/10.1016/j.tibtech.2025.01.010.

Yu, S., Plan, M.R., Winter, G., Krömer, J.O., 2016. Metabolic engineering of *Pseudomonas putida* KT2440 for the production of *para*-hydroxy benzoic acid. Front. Bioeng. Biotechnol. 4, 90. https://doi.org/10.3389/fbioe.2016.00090.

Zhang, S., Pohnert, G., Kongsaeree, P., Wilson, D.B., Clardy, J., Ganem, B., 1998. Chorismate mutase-prephenate dehydratase from Escherichia coli: study of catalytic and regulatory domains using genetically engineered proteins. J. Biol. Chem. 273 (11), 6248–6253. https://doi.org/10.1074/jbc.273.11.6248.

Zhang, S., Wilson, D.B., Ganem, B., 2000. Probing the catalytic mechanism of prephenate dehydratase by site-directed mutagenesis of the Escherichia coli P-protein dehydratase domain. Biochemistry 39 (16), 4722–4728. https://doi.org/10.1021/bi9926680.

Zobel, S., Benedetti, I., Eisenbach, L., de Lorenzo, V., Wierckx, N., Blank, L.M., 2015. Tn7-based device for calibrated heterologous gene expression in *Pseudomonas putida*. ACS Synth. Biol. 4 (12), 1341–1351. https://doi.org/10.1021/acssynbio.5b00058.